Available online at www.sciencedirect.com
ScienceDirect
Colloids and Surfaces A: Physicochem. Eng. Aspects 318 (2008) 191–198
COLLOIDS AND SURFACES A
www.elsevier.com/locate/colsurfa

Rigorous estimation of effective protein charge from experimental electrophoretic mobilities for proteomics analysis using microchip electrophoresis

Myung-Suk Chun *, Intaek Lee

Complex Fluids Research Laboratory, Energy and Environment Div., Korea Institute of Science and Technology (KIST), Seongbuk-gu, Seoul 136-791, Republic of Korea

Received 26 September 2007; received in revised form 25 November 2007; accepted 19 December 2007
Available online 5 January 2008

Abstract

Understanding of electrophoretic mobility and zeta potential is an important issue in charge characteristics of proteins for proteomics research. By exploring the electrostatic and electrokinetic principles, we presented a framework that would allow rigorous interpretations of surface zeta potential and effective charge for highly charged conditions holding the full range of buffer pH. Together with an analytic expression by considering the Henry's formula with Debye–Hückel ansatz, the zeta potential at the protein surface was evaluated from an integral expression for the electrophoretic mobility of a spherical particle on the basis of nonlinear Poisson–Boltzmann equation. Subsequently, the effective protein charge was evaluated from the corresponding relationships between potential distribution and surface charge, with accounting for the presence of an electric double layer. Applying the microchip electrophoresis, the experimental results of mobility data were obtained for model proteins with bovine serum albumin and ovalbumin in different pH of buffer solution. To illustrate the usefulness of our considerations, experimental data of electrophoretic mobility available in the literature are also included. It is evident that the results by linear correlations are identified to overestimate the zeta potential, while they underestimate the effective charge. The discrepancy between linear and nonlinear correlations is trivial for the zeta potential less than 25.69 mV, however, it fairly increases with increasing the absolute value of zeta potential.

Keywords: Electrophoretic mobility; Protein charge; Microchip electrophoresis; Electrokinetic flow; Poisson–Boltzmann equation; Zeta potential

1. Introduction

Analysis of proteins is complicated, whereas its analysis is important in order to understand proteomics and to gain more insight for the separation and identification of patterns of protein expression, binding, and protein function. Especially, the charge characteristics of a given protein provide essential information for studies arising in protein analysis. The advantages of miniaturized (or micro) total analysis systems (μTAS) are numerous and include faster analysis, high-resolving power, increased throughput, reduced waste, disposability, and the potential for on-site use.

Recently, the microchip electrophoresis technique has promisingly been used for the identification and analysis of proteins [1–3]. Based upon the merits of the μTAS, this technique is expected to be useful as a rapid and reliable means to measure the mobility and in turn the effective net charge of protein in different solution environments. In view of theoretical aspect, an in depth analysis of electrokinetic flow and transport in fluidic channels is necessary in the field of on-chip system [4–7].

In principle, the protein charge can be quantified using theoretical models that relate the electrophoretic mobility to the zeta potential with assumption of uniform charge distribution. Henry established a theoretical model of electrophoretic mobility for spherical colloids as early as 1931 [8]. Relevant previous studies were almost always confined to an analysis applying a linear correlation between the electrophoretic mobility and the zeta potential as an appropriate theoretical model [9–12]. The linear correlation is based on the linearized Poisson–Boltzmann (P–B) equation referred to as the Debye–Hückel (D–H) approximation. Accordingly, their results can be guaranteed only when the zeta potential of the particle is less than kT/e (i.e., 25.69 mV)

* Corresponding author. Tel.: +82 2 958 5363; fax: +82 2 958 5205.
E-mail address: mschun@kist.re.kr (M.-S. Chun).

0927-7757/$ – see front matter © 2008 Elsevier B.V. All rights reserved.
doi:10.1016/j.colsurfa.2007.12.046

Nomenclature

A	cross-sectional area of channel (m^2)
e	elementary charge (C)
E_n	exponential integral of order n (–)
E_x	applied electric field in axial direction (V/m)
$\boldsymbol{F}$	body force per unit volume (N/m^3)
kT	Boltzmann thermal energy (J)
n	number concentration of ion species ($1/m^3$)
$\boldsymbol{n}$	unit normal vector (–)
Q_p	effective net charge of particle (C)
r_p	hydrodynamic spherical radius of the particle (m)
v	local velocity (m/s)
V	average velocity (m/s)
x	streamwise distance (m)
z_i	valence of ion species (–)
Z	effective charge number (–)

Greek letters

ε	dielectric constant, or permittivity of buffer solution ($C^2/J\,m$)
ζ	zeta potential (V)
η	viscosity of buffer solution (Pa s)
κ	inverse EDL thickness (1/m)
μ	mobility ($m^2/s\,V$)
ρ_e	net charge density (C/m^3)
ϕ	external potential imposed by end-channel electrodes (V)
ψ	electric potential (V)

Subscripts

p	particle
w	wall

Superscripts

*	dimensionless

with a 1:1 type electrolyte system. However, it should be noted that many of proteins have a zeta potential greater than 25.69 mV in accordance with buffer solution environments. In view of this respect, it is necessary to consider the full nonlinear P–B electric field in the relation between the mobility and the zeta potential. More accurate value of the effective net charge of the protein can be estimated by using the correct limiting solution of the nonlinear P–B equation [13].

In this study, we developed a rather consistent framework that would allow the precise analysis of the zeta potential and charge characteristics of proteins by taking advantage of Henry's formula on the basis of nonlinear P–B equation. Employing the microchip electrophoresis system, electrokinetic measurements were performed with globular model proteins in different pH of buffer solution. In addition to obtaining the experimental results of mobility data, relevant literature values were presented, from which the zeta potential and effective charge were estimated. The verification of relative difference between linear and nonlinear correlations provides an explanation for the much more challenging issue on the explicit estimation of zeta potential and protein charge required in proteomics research. The complicate effects of ion relaxation and polarization arising at zeta potentials greater than kT/e have not been analyzed herein, since those issues are outside the central scope of this work.

2. Basic considerations

2.1. Electrokinetic transport in microchannel

We consider electrokinetic flows with zero imposed pressure gradient, where the streamwise electric field is positive in the direction of the positive x-axis, as illustrated in Fig. 1. The Navier–Stokes equation of motion for steady and incompressible low Reynolds number flow is given as

$$\eta\nabla^2\boldsymbol{v} = -\boldsymbol{F} \tag{1}$$

where η is the viscosity of the buffer solution, $\boldsymbol{v}$ the velocity, and $\boldsymbol{F}$ is the body force per unit volume. Applying the external potential ϕ imposed by end-channel electrodes, the action of uniform electric field $E_x = -\,d\phi(x)/dx$ on the net charge density ρ_e can be written as $F = \rho_e E_x$ [5,7,14]. According to the Poisson equation of electrostatics, the net charge density is related to the electric potential ψ

$$\rho_e = -\varepsilon\nabla^2\psi \tag{2}$$

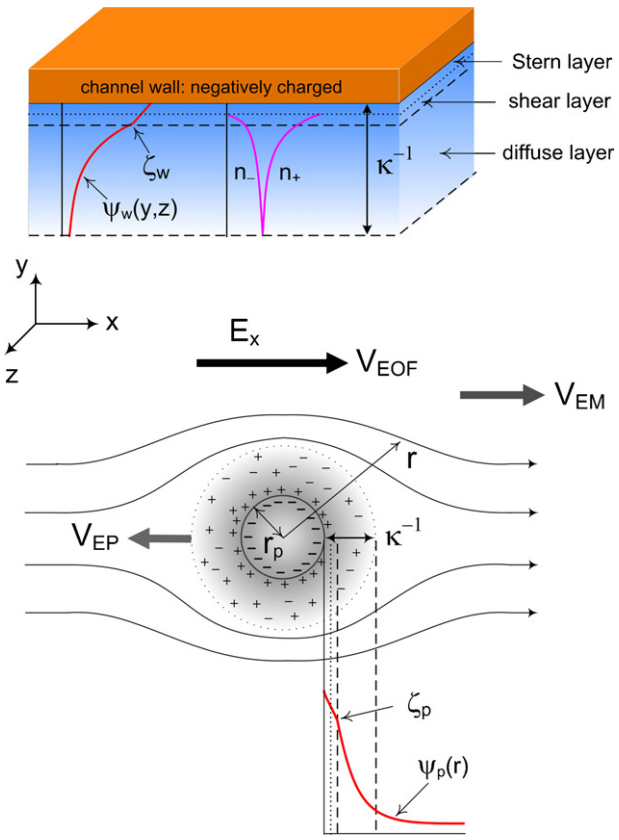

Fig. 1. Schematic of the electric potential distribution near the channel wall and the surface of an electrophoretic moving colloidal particle, where κ^{-1} corresponds to the electric double layer thickness.

where ψ depends on the transverse and spanwise positions and ε is the dielectric constant of the buffer solution given as a product of the dielectric permittivity of a vacuum ($=8.854\times10^{-12}\,C^2/J\,m$) and the relative permittivity. Both the particle surface and the channel wall are electrically nonconducting.

The electric double layer (EDL) or Debye length forms as a result of the distribution of ion charges near the dielectric and charged surface, where the EDL can be divided into an inner and a diffusive outer layer. The inner layer consists of the Stern layer and an almost immobile layer. The number concentration of ion species i ($=n_i$) follows the equilibrium Boltzmann distribution (i.e., $n_i = n_{i,\infty}\exp(-z_i e\psi/kT)$), which provides a local charge density $z_i e n_i$. Here, $n_{i,\infty}$ is the n_i far from the surface at the electroneutral state, z_i is the valence of type-i ions, e is the elementary charge ($=1.6\times10^{-19}$ C), and kT is the Boltzmann thermal energy (cf., $k=1.38\times10^{-23}$ J/K). Combining Eqs. (1) and (2) and integrating manipulations with the Dirichlet boundary condition at the channel wall and the Neumann boundary condition in the center of the channel yield the streamwise velocity profile of electroosmotic flow (EOF)

$$v_{EOF} = -\frac{\varepsilon\zeta_w E_x}{\eta}\left[1-\frac{\psi}{\zeta_w}\right] \tag{3}$$

where ζ_w indicates the zeta potential of the channel wall.

As the EDL thickness decreases, the flow rate dependence on the zeta potential becomes more linear. In the infinitely thin limit, one obtains a straight line in accordance with the Helmholtz–Smoluchowski (H–S) equation for the EOF velocity inside a microchannel of arbitrary shape, given by [15,16]

$$V_{EOF} = -\frac{\varepsilon\zeta_w E_x}{\eta}. \tag{4}$$

Here, V_{EOF} corresponds to $(1/A)\int_A v_{EOF}\,dA$ averaged over the cross-sectional area A. We note that the viscosity and permittivity are assumed as uniform and constant within the EDL. In Fig. 1, the particle is taken to have a constant electrophoretic velocity as a consequence of applying a uniform electric field E_x. From the local charge density $z_i e n_i$ for symmetric electrolytes, substitution of the net charge density ρ_e ($\equiv e\Sigma_i z_i n_i = ez(n_+ - n_-)$) into Eq. (2) leads to the P–B equation; $\nabla^2\psi = -\rho_e(\psi)/\varepsilon = \kappa^2\sinh\psi$. The EDL thickness κ^{-1} is defined as $\sqrt{\varepsilon kT/\left(e^2\sum_i n_{i,\infty}z_i^2\right)}$, where $n_{i,\infty}$ corresponds to a product of the concentration of ion species i (in moles per unit volume) and the Avogadro number.

2.2. Electrophoretic mobility

The mobility can be determined by dividing the average velocity by the streamwise electric field strength. The observed electrophoretic mobility μ_{EM} ($=V_{EM}/E_x$) of a particle is due to both its electrophoretic mobility μ_{EP} ($=V_{EP}/E_x$) plus the EOF mobility μ_{EOF} ($=V_{EOF}/E_x$), viz.

$$\mu_{EM} = \mu_{EP} + \mu_{EOF}. \tag{5}$$

Within experimental contexts, the observed electrophoretic mobility corresponds to the quantity of electromigration [12]. The electromigrations of neutrals will be equivalent to the electrophoretic mobility because they move at the same velocity as the EOF. Using the D–H solution for the potential distribution, the electrophoretic mobility can be written in the form known as the Henry equation [16],

$$\mu_{EP} = \frac{2}{3}\frac{\zeta_p\varepsilon}{\eta}f(\kappa r_p) \tag{6}$$

where ζ_p is the zeta potential of the particle and r_p is the hydrodynamic spherical radius of the particle. Over the whole range of dimensionless inverse EDL thickness (i.e., κr_p), the function f appearing in Eq. (6) is given by [17]

$$f(\kappa r_p) = \frac{3}{2}\left[1-\exp(\kappa r_p)\left\{5E_7(\kappa r_p) - 2E_5(\kappa r_p)\right\}\right]. \tag{7}$$

In Eq. (7), $E_n(\kappa r_p)$ denotes the exponential integral of order n and defined by [18]

$$E_n(\kappa r_p) = (\kappa r_p)^{n-1}\int_{\kappa r_p}^{\infty}\frac{e^{-t}}{t^n}\,dt = r_p^{n-1}\int_{r_p}^{\infty}\frac{e^{-\kappa r}}{r^n}\,dr. \tag{8}$$

According to the asymptotic properties of Eq. (6), $f=1$ for the Hückel limit ($\kappa r_p \to 0$) and $f=3/2$ for the H–S limit ($\kappa r_p \to \infty$).

Now, we consider the electrophoretic mobility predicted by Henry's formula using the nonlinear P–B equation for electric surface potential greater than kT/e. The solution is obtained for the pressure and velocity distributions about the particle illustrated as a sphere in Fig. 1. Employing this solution allows us to calculate the z component of the stress normal to any point of the surface. From Faxen's first law for creeping flow, the drag force on a sphere moving at velocity V_{EP} is obtained as $6\pi\eta r_p V_{EP}$ [14]. The electric force in the x-direction exerted on a charged sphere in a dielectric containing free charges is given by $-4\pi r_p^2\varepsilon(d\psi_p/dr)_{r=r_p}E_x$ [8]. The sum of the hydrodynamic force and the force due to the surface charge gives the total force upon the particle, and this total force must vanish for steady motion. Remarkably, Henry's result provides the following mobility expression

$$\mu_{EP} = \frac{\varepsilon\zeta_p}{\eta}\left[1-\frac{5r_p^5}{\zeta_p}\int_{r_p}^{\infty}\frac{\psi_p(r)}{r^6}\,dr + \frac{2r_p^3}{\zeta_p}\int_{r_p}^{\infty}\frac{\psi_p(r)}{r^4}\,dr\right] \tag{9}$$

where $\psi_p(r)$ denotes the electric potential at a distance r outside the particle.

2.3. Electric potential distribution and surface charge for spherical particle

The estimation of the protein charge requires the understanding of electrostatic theory. The effective net charge Q_p can be calculated from the Poisson equation for spherical particle. Because of electroneutrality, the charge on the particle surface must balance the charge in the EDL so that

$$Q_p = -\int_S \varepsilon(\boldsymbol{n}\cdot\nabla\psi)\,dS = -\int_{r_p}^{\infty}4\pi(\varepsilon\nabla^2\psi)r^2\,dr. \tag{10}$$

Integrating and letting $\partial\psi/\partial r \to 0$ as $r \to \infty$, we obtain

$$Q_p = 4\pi\varepsilon r_p^2 \nabla\psi\Big|_{r=r_p}. \quad (11)$$

For D–H approximation, introducing the linearized P–B equation with the corresponding boundary conditions provides [19]

$$\nabla^2\psi = \kappa^2\psi = \kappa^2\zeta_p\left(\frac{r_p}{r}\right)\exp\{-\kappa(r-r_p)\}. \quad (12)$$

Then, the surface charge of a sphere Q_p can be related to the zeta potential, as follows

$$Q_p = 4\pi\varepsilon r_p(1+\kappa r_p)\zeta_p. \quad (13)$$

The case of high-surface potential (i.e., $\zeta_p > kT/e$), where Eq. (9) should be applied, is much more undertaken to conduct the real situations. Under conditions for which the nonlinear correlation is valid, we introduce the formula previously derived by Ohshima [13], although detailed procedure is not described here. As a proper expression of ψ_p in Eq. (9), we can use the first order analytical solution, that is

$$\psi_p^*(r) = 2\ln\left[\left(\frac{1+Ts}{1-Ts}\right)\left(\frac{1+(T/(2\kappa r_p+1))s}{1-(T/(2\kappa r_p+1))s}\right)\right] \quad (14)$$

where

$$s = \left(\frac{r_p}{r}\right)\exp\{-\kappa(r-r_p)\}, \quad (15)$$

$$T = \tanh\left(\frac{\zeta_p^*}{4}\right)\left[\frac{1+\kappa r_p/(\kappa r_p+1)}{1+\left\{1-((2\kappa r_p+1)/(\kappa r_p+1)^2)\tanh^2(\zeta_p^*/4)\right\}^{1/2}}\right] \quad (16)$$

along with the dimensionless parameters ψ_p^* ($=\psi_p ez_i/kT$) and ζ_p^* ($=\zeta_p ez_i/kT$). It is worth noting that this analytical solution fairly coincides with the exact numerical value.

A more accurate relationship between the surface charge and the surface potential for a noninteracting sphere can be formulated by approximating the spherical nonlinear P–B equation with solvable differential equation. Under the assumption of uniform charge distribution, the effective net charge Q_p of spherical particles can be expressed in powers of $(\kappa r_p)^{-1}$ up to $O[(\kappa r_p)^{-2}]$, that is

$$Q_p = 4\pi r_p^2\alpha\sinh\left(\frac{\zeta_p^*}{2}\right)\left[1+\frac{2}{(\kappa r_p)\cosh^2\left(\zeta_p^*/4\right)}+\frac{8\ln\left\{\cosh\left(\zeta_p^*/4\right)\right\}}{(\kappa r_p)^2\sinh^2\left(\zeta_p^*/2\right)}\right]^{1/2} \quad (17)$$

where $\alpha = 2\varepsilon\kappa kT/e$. This second order ansatz yields an excellent approximation to the exact numerical results over a wide range of κr_p values for any value of the surface potential. The effective charge number of the particle Z is then calculated as Q_p/e, and therefore, it is possible to determine the value of Z from the zeta potential.

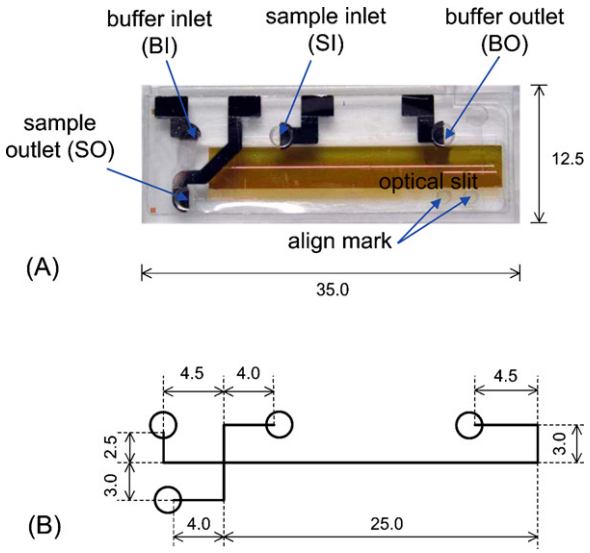

Fig. 2. (A) Electrophoresis microchip (Shimadzu Instruments, Kyoto, Japan) used in experiments, and (B) layout of dimension given in mm (cf. Ref. [21]).

3. Materials and methods

3.1. Microchip electrophoresis system

The mobility measurements were carried out using a microchip electrophoresis system MCE-2010 purchased from Shimadzu Instruments (Kyoto, Japan). The computer-controlled system consisted of a linear imaging UV detector (D_2 lamp), a four-separate power supply, a syringe unit for the introduction and evacuation of the buffer and the sample, a drive mechanism (chip tray) to move a chip to a specified position, and an autosampler. Details regarding instrumentation were described elsewhere by the manufacturer [20,21]. The UV detection by a photodiode array (PDA) located under the whole separation channel allows that progresses of particle migration can be completely recorded on the real-time basis for the total separation time.

We used the quartz microchip produced at Shimadzu Corp. employing the photolithographic, microfabrication techniques. As displayed in Fig. 2(A), the microchip had the simple cross-channel design with a sample injection channel, a separation channel, and four reservoirs at the end of each channel. The dimensions of the channel were 50 μm in depth and 110 μm in width, and the volume of every reservoir was 3 μL. The inner surface of microchannel was coated with a thin layer of linear polyacrylamide (PAA) to annihilate EOF and particle adsorption. The linear PAA is widely used for coating the surface of fused-silica and quartz, since its coating has to be hydrophilic to suppress the adhesive interaction [22,23]. Along the separation channel ranging from the cross point to the first corner, there is an optical slit at the bonding interface to cut off stray light. As shown in Fig. 2(B), the length of the separation channel was 25 mm. The incident light is cut selectively by the optical slit to eliminate the stray light, and the signal light passing through the channel is detected by the PDA, from which high sensitivity is effectively achieved [24,25].

3.2. Proteins and buffer solution

As the model proteins, bovine serum albumin (BSA) and ovalbumin (OV) were purchased from Sigma Chemical Co. (St. Louis, MO). BSA was prepared from fraction V (A-3059, 99% purity) and then crystallized and lyophilized. OV was Grade VI (A-2512, ≥98% purity) with a further purification by chromatography. It is well known that the molecular weights are 66 kDa for BSA and 44.3 kDa for OV, and their isoelectric points lie between pH 4.6 and 5.4. They have a shape of a prolate ellipsoid with the equivalent spherical radius of 3.45 nm for BSA and 2.34 nm for OV. Each protein solution of 400 ppm was prepared with the buffer solution.

Phosphate buffers with an ionic strength of 0.13 M were prepared from sodium phosphate and phosphoric acid mixed with each quantity for the desired pH. The viscosity measured by a low-shear capillary viscometer of Ubbelohde type results in 0.98 mPa s at 25 °C. Dextran of 0.04 mM (2×10^3 kDa, Sigma) was applied for the gel material, and 2 mM sodium azide was added as the bactericide needed to prevent the degeneration. Compared to the case of zone electrophoresis, the adoption of gel electrophoresis mode offers many advantages for the separation of protein mixtures. In this study, however, the proteins do not interact with the gel, since the migrating protein is small in comparison with the gel matrix through which it migrates. The pH was adjusted with 0.05 M HCl and 0.05 M KOH aqueous solutions, and we used the deionized and distilled water with a resistance of 18 MΩ cm.

3.3. Microchip operation

The potential at each reservoir and duration of voltage application were controlled by monitoring sample zone width at the cross point. Benzyl alcohol of 3 mM was prepared as a neutral marker so that the migration time for the peak gave the EOF velocity. The sample loading was performed at the field strength of 180 V/cm with 90 s by applying 420, 390, and 630 V to the sample inlet (SI) reservoir, buffer inlet (BI) reservoir, and buffer outlet (BO) reservoir, respectively, while the sample outlet (SO) reservoir was grounded (GND). For mobility measurements, potentials of 500, 1030, GND, and 500 V were applied, respectively. The applied field strength for migration was 290 V/cm, and the duration of potential application was 40 s. To measure the electromigration of proteins, the optimized potentials at SI, BI, BO, and SO were 200, 300, GND, and 500 V for sample loading, and subsequently 100, 100, 550 V, and GND for separation. All the instrument control and data acquisition were processed using the MCE-2010 software. The system automatically stopped after specified times, and then the UV absorption at each pixel was simultaneously measured for 5 s at 2-Hz intervals.

4. Results and discussion

4.1. Mobility and zeta potential of proteins

The snapshot mode of linear imaging UV detection enabled a real-time observation of migration pattern of protein samples. In

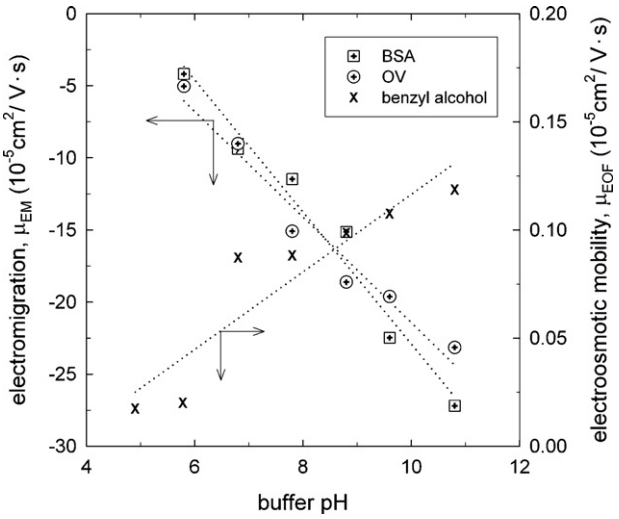

Fig. 3. The electromigration of BSA and ovalbumin (OV) and the electroosmotic flow mobility of benzyl alcohol with different buffer solution pH.

Fig. 3, the electromigration mobility of BSA as well as OV shows negative values for buffer pH larger than 5, where its magnitude increases with increasing buffer pH. For the same range of buffer pH, the EOF mobility showing positive values increases with increasing buffer pH. According to Eq. (4), the zeta potential of the channel wall is estimated −0.03 and −0.17 mV at buffer pH 4.9 and 10.8, respectively. The PAA coating reduces the magnitude of the zeta potential of the channel wall leading to a decrease in the EOF mobility, which agrees with the trend found in the literature [26]. The dissociation of ionic groups from the PAA coating is developed by the increase of buffer pH, and then anions increase in the buffer solution. Since the channel wall is negatively charged, although it is slight, the electrostatic long-range interaction is involved between the channel wall and proteins.

The electrophoretic mobility μ_{EP} is estimated by subtracting EOF mobility from electromigration, as given in Eq. (5). The buffer solution of the present study at 25 °C is identified as a condition with the inverse EDL thickness κ of 1.2 nm^{-1}, ensuring that κr_p values for BSA and OV result in the region between the two limiting cases in the Henry's formula. In Fig. 4(A) and (B), comparisons are shown between the published and the present data of μ_{EP} for BSA and OV. A many literature data for various globular proteins were obtained, for instance, by applying the particle electrophoresis cell [9,27], moving boundary technique [28], free-flow electrophoresis cell [9], and fused-silica capillary electrophoresis [11]. Note that the buffer conditions of total ionic strength are different as 0.02 M sodium acetate [9], 0.01 M sodium chloride [11], and 0.1 M with different buffer ions depending on the pH range [27,28]. Similar to the results of electromigration, the absolute values of μ_{EP} increase with increasing buffer pH. Although the general trend of the data is evident, the discrepancies between the various published sources and between these and our present results are evident. These discrepancies can be attributed to two main factors, viz. the effect of different buffer condition and the method of measurement.

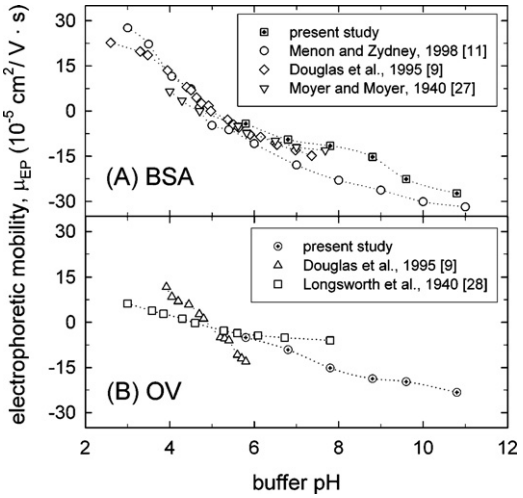

Fig. 4. The electrophoretic mobility of proteins with different buffer solution pH: (A) BSA and (B) ovalbumin (OV).

From the μ_{EP} data, we estimated the zeta potential of proteins from both an analytic expression for the mobility by considering the Henry's formula with D–H approximation as well as an integral expression on the basis of nonlinear P–B equation, and then compared two results. The exact values of zeta potential based on the linear correlation can be estimated by using Eqs. (6)–(8), which should be applicable for the whole range of κr_p. The exponential integrals were evaluated by utilizing Mathematica (http://mathworld.wolfram.com). For the zeta potential based on the nonlinear correlation, Eq. (9) is solved for zeta potential numerically using Brent's method. The integrals on the right-hand side of Eq. (9) are evaluated using Romberg integration on an open interval as implemented in Numerical Recipes [29]. As mentioned earlier, the electric potential profile $\psi_p(r)$ in Eq. (9) is represented by Eq. (14).

In Fig. 5, the values of the isoelectric points are found in the range of roughly pH 4.5–5 for BSA. Present results of the zeta potentials are negative throughout the entire pH range tested (ca. pH 5–11). The results by linear correlation are shown to overestimate the zeta potential, even if the difference is not severe. The difference between two results determined by linear and nonlinear correlations becomes larger as the pH increases, which gives rise to a change in the zeta potential of above kT/e. This actual dependency of the pH upon the difference indicates the need of an explicit estimation and a clear limitation of the linear correlation with D–H approximation. The result of OV is in qualitative agreement, although its figure is not provided here. Since the absolute value of the zeta potential of OV is less than about 40 mV, it can be expected that the relative difference between linear and nonlinear correlations is less considerable.

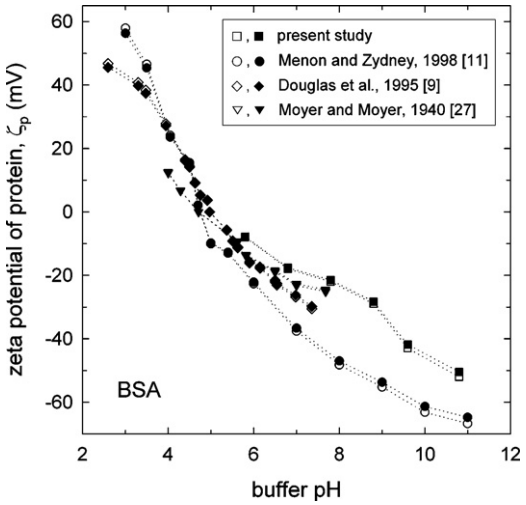

Fig. 5. Estimated zeta potentials of BSA computed from both D–H (open symbols) as well as nonlinear P–B equations (closed symbols) as a function of buffer solution pH.

4.2. Effective net charge estimations

In order to access the need of nonlinear correlation, the effective charge number Z of BSA was estimated from the zeta potential ζ_p obtained by the D–H as well as nonlinear P–B equations. We obtained three kinds of values of the effective charge number: Z_{D-H}^{D-H} from full linear correlations for ζ_p as well as Z, Z_{P-B}^{P-B} from full nonlinear correlations for ζ_p as well as Z, and Z_{D-H}^{P-B} from nonlinear correlation for ζ_p and linear correlation for Z. The linear and nonlinear correlations between ζ_p and Z were accomplished by using Eqs. (13) and (17), respectively. The ellipsoidal shape of the globular BSA was represented by the spherical model with equivalent radius. Fig. 6(A) and (B) show that the values of Z_{P-B}^{P-B} based on the full nonlinear correlations for ζ_p as well as Z have higher absolute values than the values of either Z_{D-H}^{D-H} or Z_{D-H}^{P-B} and this trend becomes more significant with increasing buffer pH. The discrepancy results from the nonlinear electrostatic effect, which has been neglected in the linearized version of P–B equation used in Eqs. (6) and (13). It can be observed that the discrepancy in Fig. 6(B) is larger than that in Fig. 6(A).

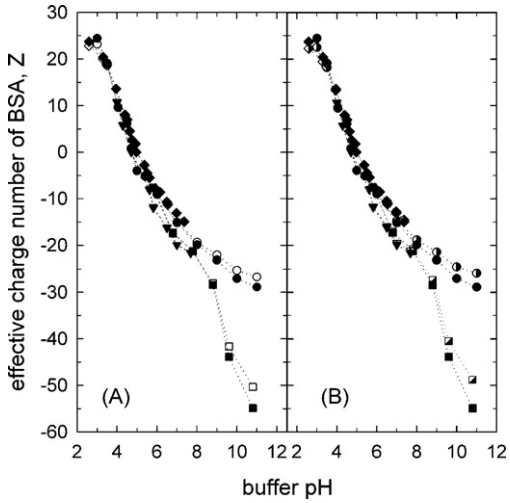

Fig. 6. The effective charge number of BSA vs. buffer solution pH: (A) estimations from nonlinear correlations for both ζ_p and Z (closed symbols) and from linear correlations for both ζ_p and Z (open symbols), and (B) estimations from nonlinear correlations for both ζ_p and Z (closed symbols) and from nonlinear correlation for ζ_p and linear correlation for Z (semi-open symbols). Symbols have the same meaning in the case of Fig. 5.

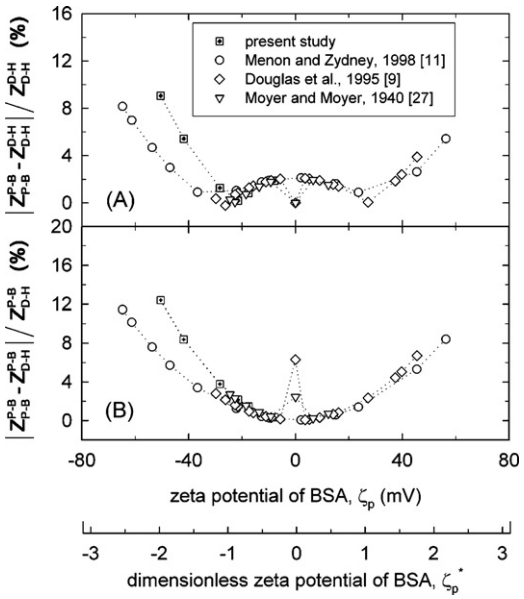

Fig. 7. The relative differences in estimated values of effective charge number: (A) between purely nonlinear and purely linear correlations, and (B) between purely nonlinear and partially nonlinear correlations.

As shown in Fig. 7(A) and (B), each discrepancy could be quantified as the relative differences in estimated values of effective charge number. As long as the zeta potential is low (i.e., $|\zeta_p| \leq kT/e$), the relative difference with respect to an underestimation in the effective net charge is less than about 3% indicating that Henry's mobility formula is still good approximate expression. However, the relative difference increases more than twice once the zeta potential becomes $2kT/e$. In any case, it should be pointed out that the increase of the relative difference in effective charge estimation is predominant as the zeta potential further increases. Therefore, the nonlinear correction is obviously necessary for the accurate analysis of proteins when the zeta potential of proteins is greater than kT/e.

5. Conclusions

The microchip electrophoresis has been demonstrated to be applicable to the measurement of accurate electrophoretic mobility over a wide range of buffer pH. It requires extremely small amounts of protein (cf., nanoliter volumes), making it very suitable for protein characterization that exploit differences in electrostatic interactions.

Despite of the variant buffer conditions in ionic strength and/or composition, our experimental results of the mobility could be compared with the literature values for globular proteins. Both the zeta potential and the effective net charge were estimated from the mobility data obtained at different buffer pH. The trivial relative difference with respect to an underestimation in the effective net charge, for the case of low zeta potential ($|\zeta_p| \leq kT/e$), indicates conventional Henry's mobility formula is still valid. Once the zeta potential of BSA becomes greater than about $3kT/e$, however, the relative difference of underestimation in the effective charge appears more than 20%, and its value subsequently increases as the zeta potential increases. Although the nonlinear correlation what we conducted here is partly inconvenient for practical calculations, it is applicable to the rigorous estimation of zeta potential as well as effective charge for all values of zeta potential.

Acknowledgements

The authors would like to thank interim research student D.Y. Kim for assisting the operation of MCE apparatus. This work was supported by the Basic Research Fund (R01-2004-000-10944-0) from the Korea Science and Engineering Foundations (KOSEF) as well as the Future-Oriented μTAS Research Fund (2E19690) from the Korea Institute of Science and Technology (KIST) provided to M-SC.

References

[1] D.J. Harrison, K. Fluri, K. Seiler, Z. Fan, C.S. Effenhauser, A. Manz, Micromachining a miniaturized capillary electrophoresis-based chemical analysis system on a chip, Science 261 (1993) 895.
[2] L.J. Jin, B.C. Giordano, J.P. Landers, Dynamic labeling during capillary or microchip electrophoresis for laser-induced fluorescence detection of protein-SDS complexes without pre- or postcolumn labeling, Anal. Chem. 73 (2001) 4994.
[3] H. Nagata, M. Tabuchi, K. Hirano, Y. Baba, Microchip electrophoretic protein separation using electroosmotic flow induced by dynamic sodium dodecyl sulfate-coating of uncoated plastic chips, Electrophoresis 26 (2005) 2247.
[4] C. Rice, R. Whitehead, Electrokinetic flow in a narrow cylindrical capillary, J. Phys. Chem. 69 (1965) 4017.
[5] M.-S. Chun, T.S. Lee, N.W. Choi, Microfluidic analysis on electrokinetic streaming potential induced by microflows of monovalent electrolyte solution, J. Micromech. Microeng. 15 (2005) 710.
[6] D.P.J. Barz, P. Ehrhard, Model and verification of electrokinetic flow and transport in a micro-electrophoresis device, Lab Chip 5 (2005) 949.
[7] S. Pennathur, J.G. Santiago, Electrokinetic transport in nanochannels. 1. Theory, Anal. Chem. 77 (2005) 6772.
[8] D.C. Henry, The cataphoresis of suspended particle. Part I. The equation of cataphoresis, Proc. Royal Soc. London, A 133 (1931) 106.
[9] N.G. Douglas, A.A. Humffray, H.R.C. Pratt, G.W. Stevens, Electrophoretic mobilities of proteins and protein mixtures, Chem. Eng. Sci. 50 (1995) 743.
[10] J. Gao, G.M. Whitesides, Using protein charge ladders to estimate the effective charges and molecular weights of proteins in solution, Anal. Chem. 69 (1997) 575.
[11] M.K. Menon, A.L. Zydney, Measurement of protein charge and ion binding using capillary electrophoresis, Anal. Chem. 70 (1998) 1581.
[12] F. Omasu, Y. Nakano, T. Ichiki, Measurement of the electrophoretic mobility of sheep erythrocytes using microcapillary chips, Electrophoresis 26 (2005) 1163.
[13] H. Ohshima, T.W. Healy, L.R. White, Accurate analytic expressions for the surface charge density/surface potential relationship and double-layer potential distribution for a spherical colloidal particle, J. Colloid Interf. Sci. 90 (1982) 17.
[14] J.H. Masliyah, S. Bhattacharjee, Electrokinetic and Colloid Transport Phenomena, John Wiley & Sons, Hoboken, 2006.
[15] S. Ghosal, Electrokinetic flow and dispersion in capillary electrophoresis, Annu. Rev. Fluid Mech. 38 (2006) 309.
[16] W.B. Russel, D.A. Saville, W.R. Schowalter, Colloidal Dispersions, Cambridge University Press, New York, 1989.
[17] H. Ohshima, A simple expression for Henry's function for the retardation effect in electrophoresis of spherical colloidal particles, J. Colloid Interf. Sci. 168 (1994) 269.
[18] H. Jeffrey, B.S. Jeffrey, Methods of Mathematical Physics, 3rd ed., Cambridge University Press, New York, 1988.

[19] M.-S. Chun, W.R. Bowen, Rigorous calculations of linearized Poisson–Boltzmann interaction between dissimilar spherical colloids and osmotic pressure in concentrated dispersions, J. Colloid Interf. Sci. 272 (2004) 330.
[20] Z. Xu, T. Ando, T. Nishine, A. Arai, T. Hirokawa, Electrokinetic supercharging preconcentration and microchip gel electrophoretic separation of sodium dodecyl sulfate–protein complexes, Electrophoresis 24 (2003) 3821.
[21] F. Xu, M. Jabasini, B. Zhu, L. Ying, X. Cui, A. Arai, Y. Baba, Single-step quantitation of DNA in microchip electrophoresis with linear imaging UV detection and fluorescence detection through comigration with a digest, J. Chromatogr. A 1051 (2004) 147.
[22] S. Hjertén, High-performance electrophoresis: Elimination of electroendosmosis and solute adsorption, J. Chromatogr. 347 (1985) 191.
[23] V. Dolnik, Wall coating for capillary electrophoresis on microchips, Electrophoresis 25 (2004) 3589.
[24] H. Nakanishi, T. Nishimoto, A. Arai, H. Abe, M. Kanai, Y. Fujiyama, T. Yoshida, Fabrication of quartz microchips with optical slit and development of a linear imaging UV detector for microchip electrophoresis systems, Electrophoresis 22 (2001) 230.
[25] S. Suzuki, Y. Ishida, A. Arai, H. Nakanishi, S. Honda, High-speed electrophoretic analysis of 1-phenyl-3-methyl-5-pyrazolone derivatives of monosaccharides on a quartz microchip with whole-channel UV detection, Electrophoresis 24 (2003) 3828.
[26] B.J. Kirby, A.R. Wheeler, R.N. Zare, J.A. Fruetel, T.J. Shepodd, Programmable modification of cell adhesion and zeta potential in silica microchips, Lab Chip 3 (2003) 5.
[27] L.S. Moyer, E.Z. Moyer, Electrokinetic aspects of surface chemistry. VII. The electrokinetic behavior of microscopic particles in the presence of horse, human or rabbit serum, J. Biol. Chem. 132 (1940) 373.
[28] L.G. Longsworth, R.K. Cannan, D.A. MacInnes, An electrophoretic study of the proteins of egg white, J. Am. Chem. Soc. 62 (1940) 2580.
[29] W.H. Press, B.P. Flannery, S.A. Teukolsky, W.T. Vetterling, Numerical Recipes, Cambridge University Press, New York, 1986.